ONE-DIMENSIONAL qP-WAVE VELOCITY MODEL OF THE UPPER CRUST FOR THE WEST BOHEMIA/VOGTLAND EARTHQUAKE SWARM REGION

J. MÁLEK[1], J. HORÁLEK[2] AND J. JANSKÝ[3]

1 Institute of Rock Structure and Mechanics, Acad. Sci. Czech Republic, V Holešovičkách 41, 182 09 Prague 8, Czech Republic (malek@irsm.cas.cz)

2 Geophysical Institute, Acad. Sci. Czech Republic, Boční II/1401, 141 31 Prague 4, Czech Republic (jhor@ig.cas.cz)

3 Department of Geophysics, Faculty of Mathematics and Physics, Charles University, Ke Karlovu 3, 121 16 Prague 2, Czech Republic (jansky@seis.karlov.mff.cuni.cz)

Received: August 24, 2001; Revised: November 18, 2004; Accepted: January 23, 2005

ABSTRACT

The western part of the Bohemian Massif (West Bohemia/Vogtland region) is characteristic in the relatively frequent recurrence of intraplate earthquake swarms and in other manifestations of past-to-recent geodynamic activity. In this study we derived 1D anisotropic qP-wave model of the upper crust in the seismogenic West Bohemia/Vogtland region by means of joint inversion of two independent data sets - travel times from controlled shots and arrival times from local earthquakes extracted from the WEBNET seismograms. We derived also simple 1-D P-wave and S-wave isotropic models. Reasons for deriving these models were: (a) only simplified crustal velocity models, homogeneous half-space or 1D isotropic layered models of this region, have been derived up to now and (b) a significant effective anisotropy of the upper crust in the region which was indicated recently by S-wave splitting. Both our anisotropic qP-wave and isotropic P-and S-wave velocity models are constrained by four layers with the constant velocity gradient. Weak anisotropy for P-waves is assumed. The isotropic model is represented by 9 parameters and the anisotropic one is represented by 24 parameters. A new robust and effective optimization algorithm - isometric algorithm - was used for the joint inversion. A two-step inversion algorithm was used. During the first step the isotropic P- and S-wave velocity model was derived. In the second step, it was used as a background model and the parameters of anisotropy were sought.

Our 1D models are adequate for the upper crust in the West Bohemia/Vogtland swarm region up to a depth of 15 km. The qP-wave velocity model shows 5% anisotropy, the minimum velocity in the horizontal direction corresponds to an azimuth of 170°. The isotropic model indicates the V_P/V_S ratio variation with depth. The difference between the hypocentre locations based on the derived isotropic and anisotropic models was found to be several hundreds of meters.

Keywords: West Bohemia/Vogtland region, earthquake swarm, anisotropy, 1D velocity model, inverse problem, earthquake location

1. INTRODUCTION

The West Bohemia/Vogtland region, covering the Czech-German border area (Fig. 1), belongs to one of the most interesting regions in Central Europe from the point of view of past-to-present geodynamic activity. One of its most spectacular geodynamic features are the periodically occurring intraplate earthquake swarms. The whole epicentral region covers an area of about 5000 km^2. The last intensive swarm with more than 8000 recorded events with maximum magnitude $M_L = 4.6$ occurred between December 1985 and January

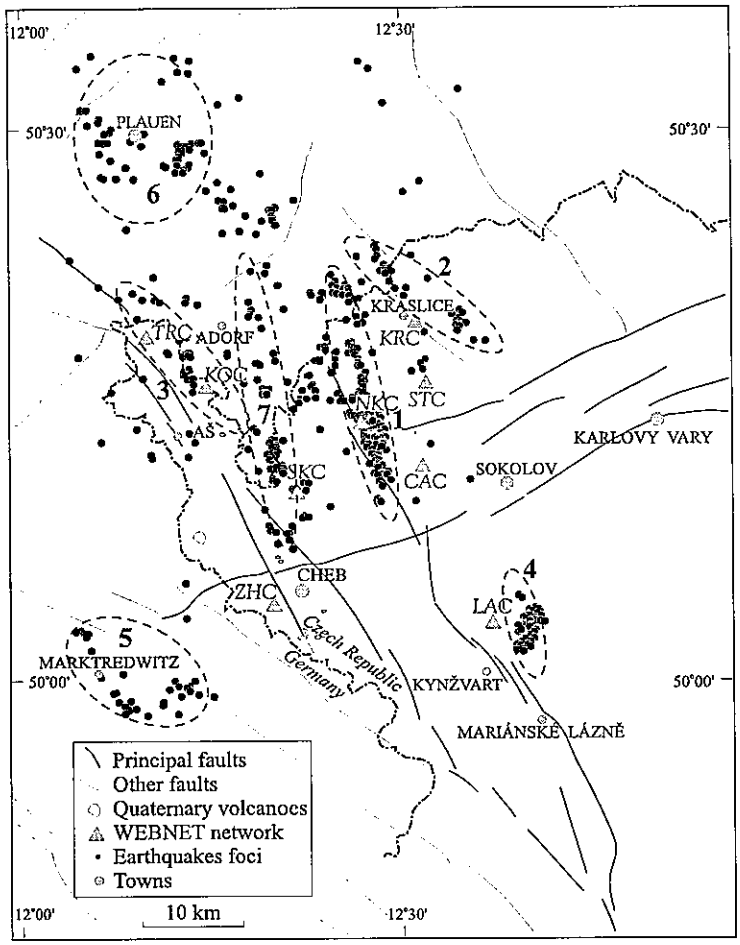

Fig. 1. Distribution of micro-earthquake epicentres located in the West Bohemia/Vogtland region in period 1991–1999. The foci locations were calculated by the FASTHYPO program using the WB95 model. The P- and S-wave onset times were extracted from the WEBNET seismograms. Focal Zones 1 through 7 are marked by dotted ellipses.

1986 (*Neunhöfer and Güth, 1989*), the recent swarm, between August and November 2000, included more than 20 000 $M_L \leq 3.4$ events (*Fischer, 2003*). Micro-earthquake activity, mostly of a swarm-like character, persists between consecutive more intensive swarms in the region. Altogether ten micro-earthquake swarms with the $M_{Lmax} > 1.5$ events occurred in the period between the 1985/86 and the 2000 earthquake swarms. Epicentres are clustered predominantly in seven main epicentral zones (Fig. 1). The depths of hypocentres are between 4 and 23 km depending on the epicentral zone, however, most of the events have been located at depths between 8 and 11 km (*Horálek et al., 2000*).

Other geophysical phenomena indicating a recent geodynamic activity of the region are vertical motions of the upper crust in the seismically active area (*Mrlina, 2000*), negative gravity anomalies (*Švancara et al., 2000*), smaller Moho depth (*Bucha and Blížkovský, 1994*), and possible updoming of the asthenosphere (*Babuška and Plomerová, 1987*). Moreover, an anomalous content of mantle-derived ^{3}He in groundwaters and a high magmatic CO_2 flux were detected there (*Heinicke and Koch, 2000; Bräuer et al., 2003*).

The West Bohemia/Vogtland region is situated in the western part of the Bohemian Massif at the contact of three principal tectonic units: the Saxothuringian, the Teplá-Barrandean Unit and the Moldanubian. Its geological structure is rather complex. The region is intersected by an ENE-WSW striking neotectonic structure, the Ohře (Eger) Graben (EG), and by the NNW-SSW striking Mariánské Lázně fault (MLF). According to *Špičák (2000)*, the EG created intrusion channels for Variscan granitoid massifs and, during the Alpine orogeny, their reactivation resulted in the formation of Tertiary basins accompanied by extensive alkaline volcanism. The Cheb Basin, 25 by 15 km in size, filled with Tertiary sediments of up to 300m thickness, is situated roughly in the centre of the region. Drillings indicate that the depth of the crystalline basement varies laterally to a fair extent.

The stress tensor estimations obtained by focal mechanism inversion (*Wirth et al., 2000; Havíř, 2000; Plenefisch and Klinge, 2003*) indicate that the crustal stress field in the West Bohemia/Vogtland region does not differ substantially from the general stress field in Central Europe, which is characterized by an SE-NW orientation of the maximum and an SW-NE orientation of the minimum horizontal axis of compression.

On account of the complexity of the geological structure, deriving realistic seismic models of the upper crust of the region is rather difficult. Moreover, seismic data available (travel times from controlled sources, arrival times from local earthquakes and from quarry blasts) are still insufficient for a 3D inversion both for small amount of data and the uneven coverage of the region. A few authors tried to construct a 3D velocity model of the region, but they were not fully successful; some causes of the failure are discussed in *Klimeš (1995)*. A general 2D P-wave velocity model of the crust along the MVE-90 (East) DEKORP profile (length of 170 km) down to MOHO was derived by *Behr et al. (1994)* using travel times of P_g and PMP-waves, and envelopes of irregular quasi-reflected wave groups. Furthermore, a number of simplified 1D velocity models adequate for individual studies (above all for purposes of earthquake location) have been derived using various kind and quality of data (local earthquakes quarry blasts, deep seismic sounding). Some of the authors restricted themselves to homogeneous half-space models, others derived layered models. Most of those models are reviewed in *Novotný (1996)*. He further

employed relevant data published previously and compiled layered crust and upper mantle model of the West Bohemia/Vogtland region WB95 (see Fig. 5). Thus, the WB95 model represents a synthesis of different 1D models of the area under study. *Janský et al. (2000)* and *Málek et al. (2000)* constructed, respectively, homogeneous and piece-wise constant gradient P- and S-velocity models for four subregions (epicentral zones 1, 2, 4 and 7 in Fig. 1). The results show that the models of the individual epicentral zones differ from one another in both P-wave velocity and V_P/V_S ratios. The differences are mostly larger in the upper parts, down to depths of about 4 km. *Málek et al. (2004)* and *Novotný et al. (2004)* found that characteristic features of 1D models of the region under study are relatively low P-wave velocities close to the surface and prominent velocity increases within the uppermost crust down to depth of about 1 km.

The anisotropy of the upper crust in the region was indicated by *Vavryčuk (1993)* who interpreted the S-wave splitting in local earthquake seismograms. In that case the medium was approximated by a transversely isotropic model with a horizontal axis of rotation and 6% S-wave anisotropy, the direction of the fast shear wave axis was estimated N31°E.

A one-dimensional anisotropic velocity model may enable more accurate hypocentre locations of local earthquakes than isotropic models, which were used for routine location so far. Moreover, the application of anisotropy, if existing, will significantly influence the response of the medium (Green's function), which is necessary for focal mechanism determination and for many other purposes.

Such issues motivated us to estimate the P-wave upper crust anisotropy using available high-quality data from controlled sources and local earthquakes. The aim of the present study is to derive proper one-dimensional isotropic P- and S-wave and anisotropic qP-wave velocity models of the upper crust for the West Bohemia/Vogtland earthquake swarm region and furthermore, to evaluate the errors in hypocentre locations resulting from neglecting anisotropy in the velocity model.

2. DATA USED

To derive the velocity models, two data sets from different sources - (1) travel times from controlled sources and (2) arrival times from local earthquakes determined from the WEBNET seismograms - were jointly inverted.

(1) The first data set included 181 P_g-wave travel times obtained from 15 controlled shots which were fired at seismic profiles A/89, B/89, C/91, D/91 and MVE/90, respectively, in West Bohemia and in the border area of Germany in 1989–1991 (*Bucha et al., 1992*). The shots were recorded by 34 digital stations (Lennartz MARS 88 and PCM 5800) deployed in West Bohemia at various epicentral distances and azimuths (Fig. 2). The frequency response of the stations was flat for the ground velocity in the 1.0–45 Hz frequency band; the sampling rate was 125 Hz. Origin times of the shots were measured with an accuracy better than 3 ms. Only clear and reliably determined onsets with an accuracy better than 16 ms (i.e. two samples) were taken into account. The shortest and the longest epicentral distance were 4 km and 39 km, respectively. The resulting 181 rays (strictly speaking their horizontal projections) provided a fair, homogeneous coverage of

the most seismically active part of the West Bohemia/Vogtland swarm region in an area of 30 by 30 km, (see Fig. 2).

(2) The second data set comprised 424 P- and 320 S-wave arrival times (only direct P and S waves were taken into account) of 65 local micro-earthquakes recorded by nine seismic stations of the WEBNET network in the period 1996–1999 (Fig. 3). The frequency response of the WEBNET seismographs is flat for the ground velocity in the 0.5–60 Hz frequency band, the sampling is 250 Hz (for more information about WEBNET refer to *Horálek et al., 2000*). The events used were selected according to the following criteria: (a) recorded at five stations at least;

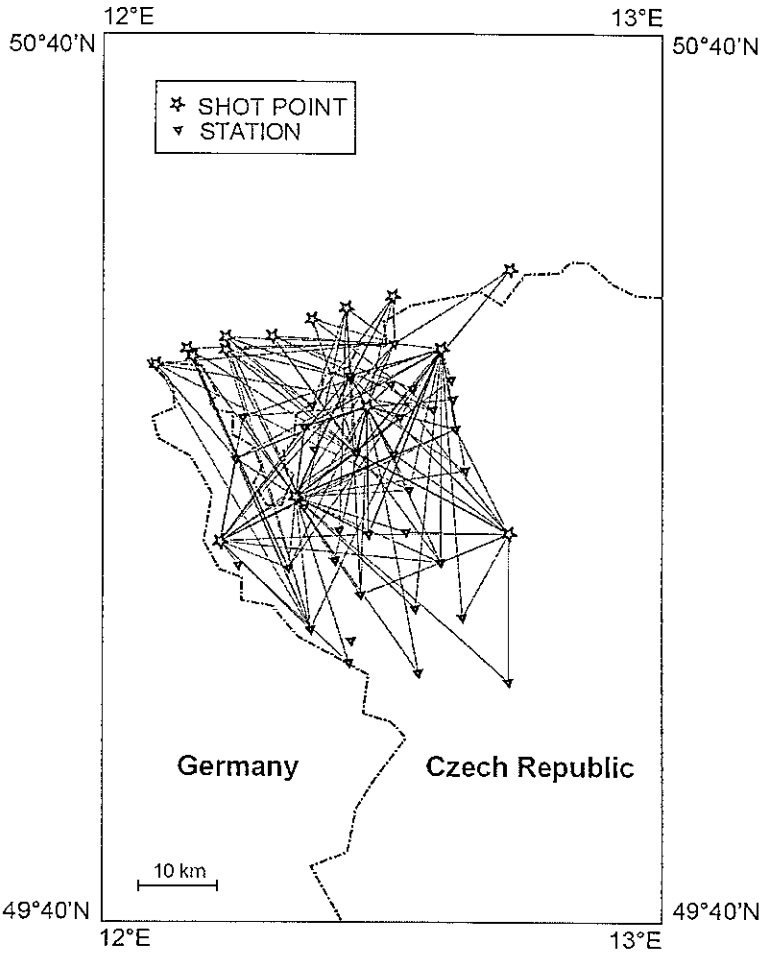

Fig. 2. Coverage of the West Bohemia/Vogtland swarm region by 181 measurements of P-wave travel times from 15 controlled shots to digital stations deployed in the region. Lines connecting the shot points with the stations depict the epicentral distances and the wave propagation directions. The measurements cover an area of about 900 km^2.

(b) the onset times determined with an accuracy of 8 ms for P-waves (i.e. two samples) and 20 ms for S-waves (i.e. five samples); (c) a homogeneous azimuthal coverage of the region by rays. The selected events covered not only Focal Zones 1, 2, 3, 4 and 7 (Fig. 1), but also the region in between. The epicentral distances ranged from a few hundred metres to 34 km; the rays covered approximately the same area as those of the shots. All the P- and S-wave arrival times were picked manually with help of particle motion analysis.

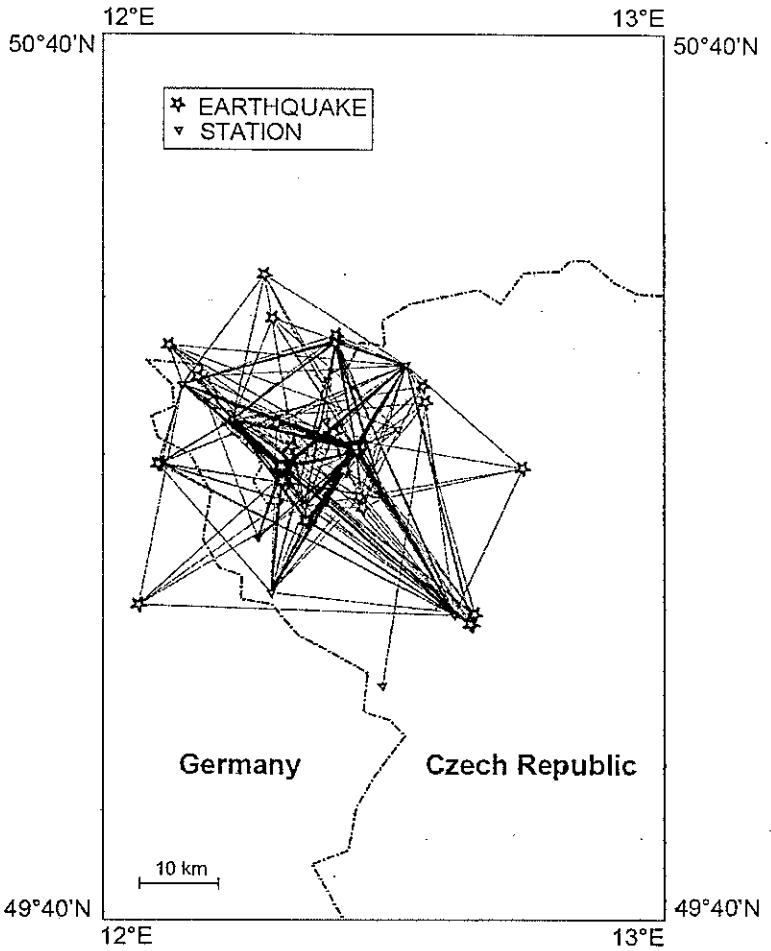

Fig. 3. Analogously as in Fig. 2 for 424 P-and 320 S-wave onsets of 65 microearthquakes extracted from the WEBNET seismograms. Rays are marked by lines connecting epicenters with stations. Note that the microearthquake observations and the travel-time measurements from the profile shots cover approximately the same area.

The whole onset time error σ equals the sum of the reading error and the velocity model error. The latter is expected to increase with epicentral distance, it is assumed to be 1% of the travel time. Weights proportional to $1/\sigma^2$ were assigned to each P- and S-onset time used in the inversion according to the estimated errors σ.

3. CONSTRAINT OF THE VELOCITY MODELS

In order to reduce the number of parameters calculated in the inversion, we constrained our model in using a piece-wise constant gradient model consisting of four layers. Thus, the gradients of velocities are constant in the individual layers and velocity jumps are not allowed at the layer boundaries. The four layers constraint resulted from preparatory tests, which showed that already three layers have a good chance of minimising the sum of travel-time residuals at locations in the 1D isotropic model. Let us emphasise that four layers are only used as an approximation of the velocity model with a variable gradient and are not directly related to the real geological structure of the upper crust in the region.

Besides, the following three parameters (for the isotropic model) were fixed: (1) the bottom of the fourth layer (z_5) at the depth of 32 km, which was estimated as the depth of the Moho discontinuity, (2) the P-wave velocity of 7.2 km/s (v_{p5}) just above the Moho (*Novotný, 1996*), and (3) the P-wave velocity of 3.7 km/s (v_{p1}) at the surface ($z_1 = 0$), which was determined using shot travel times distance of up to 1 km. In this way the isotropic velocity model is defined for inversion by 9 independent parameters: Three of them, z_2, z_3, z_4, represent the depths of boundary between the layers, (see Fig. 4), the other six parameters, v_{p2}, v_{s2}, v_{p3}, v_{s3}, v_{p4}, v_{s4}, represent the P- and S-wave velocities at the top of the second, third and fourth layers. Provided that no velocity jumps are at the layer boundaries, the velocities at the bottom of the i-th layer are equal to the velocity at the top

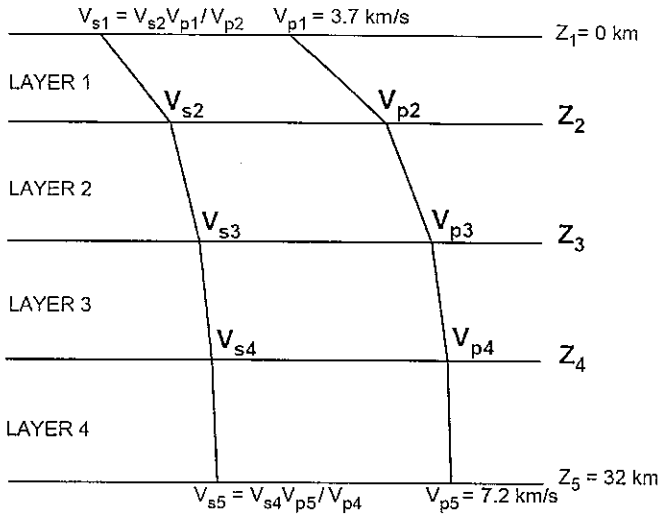

Fig.4. Constrain of the P- and S- wave isotropic model. Model parameters are in bold.

of the $(i+1)$st layer. In this way, the P- and S-wave velocities in the individual layers are represented by the equations:

$$\alpha(z) = v_{Pi} + \gamma_i (z - z_i), \text{ and } \beta(z) = v_{Si} + \xi_i (z - z_i).$$

Here, v_{Pi} and v_{Si} are the P and S velocities at the top of the i-th layer, and γ_i and ξ_i denote the P- and S-wave velocity gradient, respectively.

Since only P velocities v_{p1} (3.7 km/s) and v_{p5} (7.2 km/s) are fixed, respectively, at the top of the 1st and at the bottom of the 4th layer, we assume that $v_{s1} = v_{s2} v_{p1} / v_{p2}$ and $v_{s5} = v_{s4} v_{p5} / v_{p5}$, i.e. constant v_p/v_s ratios in layers 1 and 4. Thus, a linear variability of v_p/v_s with depth is allowed only in the 2nd and 3rd layers. Since all earthquakes taken into account were located at depths of 15 km or less, and the epicentral distances were 40 km or less, the rays taken into consideration do not propagate beneath a depth of 15 km.

As regards the anisotropy of the upper crust, only weak P-wave anisotropy was assumed, therefore, description of P-wave phase velocity in a weakly anisotropic medium according to *Pšenčík and Gajewski (1998)* was used (Appendix A). In order to reduce number of parameters sought in the inversion procedure, only the P-wave anisotropy uniform in all four layers was considered. In this way, the P-wave anisotropy is represented by 15 coefficients.

The lower accuracy and smaller number of the S-onset time readings does not enable us to search for the S-wave anisotropy, nevertheless, the S-wave onset times are used for hypocentre locations performed in the inversion.

4. INVERSION AND RESULTS

All data were jointly inverted using Isometric Method by *Málek (1997)* (see Appendix B). The parameters of the model were sought iteratively, the hypocentre coordinates of micro-earthquakes were computed in each iteration during the inversion. Models which are considered as optimal yield the minimum average travel-time residuum for both data sets weighted proportional to $1/\sigma^2$.

The anisotropic model was calculated in two steps. First, we derived a 1D isotropic P- and S-wave velocity model defined by 9 parameters. Subsequently, we used the 1D isotropic P-wave velocity model as the background model and 15 parameters describing the P-wave anisotropy were sought.

The hypocentre locations, determined by means of the isotropic model, were used in the starting model for the relocation when the parameters of the qP-wave velocity model were sought. Although the errors of the S-onsets are 2.5 times larger than those of the P-onsets and, consequently, the weights of the S-waves are 6.25 times smaller in the locating procedure, the S-onset times were also used for calculating the qP-wave model parameters, since they stabilized a locating procedure considerably and made it more efficient.

Two-point ray tracing and the formulas for the isotropic layered medium with constant gradients (*Janský, 1969*) were used. The same formulas were also used for computing the

travel times in the anisotropic medium, under the assumption that the ray paths in a weakly anisotropic medium are the same as in the isotropic medium, and only the velocity along the rays varies in dependence of directions.

The parameters of the isotropic P- and S-wave model and anisotropic qP-wave model are summarized in Table 1, dependence of the P- and S-wave velocities with depth are depicted in Fig. 5. The highest increase of the v_p and v_s is in the shallowest part to depths of about 2.5 km. The P- and S-velocity gradients are $\gamma_1 = 4.073$ km/s/km, $\gamma_2 = 0.215$ km/s/km, and $\xi_1 = 2.390$ km/s/km, $\xi_2 = 0.200$ km/s/km in the first and second layers, while $\gamma_3 = 0.049$ km/s/km, $\gamma_4 = 0.047$ km/s/km, and $\xi_3 = 0.0017$ km/s/km, $\xi_4 = 0.027$km/s/km in the third and fourth layers. Moreover, the inversion yields the values of the v_p/v_s ratio, which varies with depth. The dependence of anisotropy of the qP-wave phase velocity on the azimuth ϕ and incidence angle θ is shown in Fig. 6. The velocity in the fast direction is about 5% higher than the velocity in the slow direction, the direction of the lowest velocity in the horizontal plane is oriented approximately in the N-S direction.

Table 1. Model parameters for isotropic and anisotropic models.

Isotropic P- and S-wave background model	
z_1 [km]	0.0 (surface)
z_2 [km]	0.41
z_3 [km]	2.46
z_4 [km]	8.41
v_{P1}/v_{S1} [km/s]	3.70/2.18 = 1.70
v_{P2}/v_{S2} [km/s]	5.37/3.16 = 1.70
v_{P3}/v_{S3} [km/s]	5.81/3.57 = 1.63
v_{P4}/v_{S4} [km/s]	6.10/3.58 = 1.70
Anisotropic coefficients	
ε_x	−0.012
ε_y	0.007
ε_z	0.011
δ_x	−0.004
δ_y	0.006
δ_z	−0.005
χ_x	0.009
χ_y	−0.004
χ_z	0.001
ε_{15}	0.002
ε_{16}	0.007
ε_{24}	0.003
ε_{26}	0.007
ε_{34}	−0.007
ε_{35}	−0.005

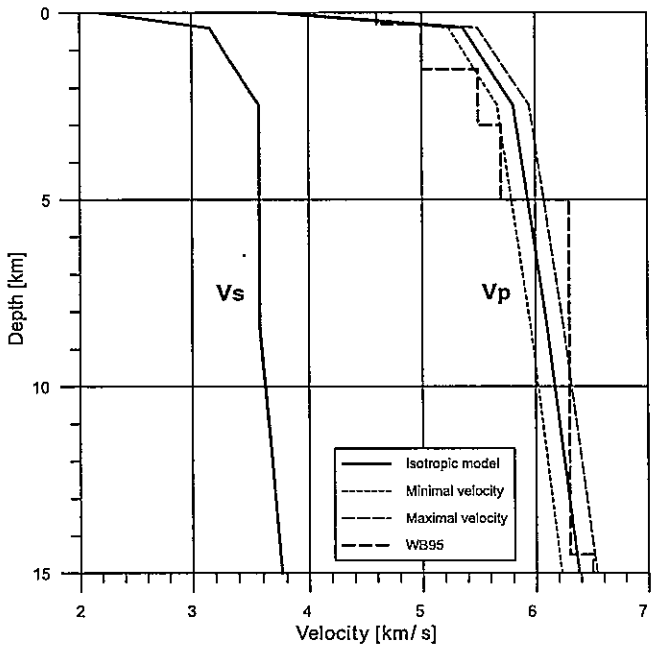

Fig. 5. Velocity-depth isotropic P and S models and velocities in the minimum and maximum directions in the qP model. The WB95 model, which represents a synthesis of different 1D models of the area under study, is shown for comparison.

The locations of hypocentres in isotropic and anisotropic models differ, the shift of the hypocentres (z_{ani}–z_{iso} - in depth, Δr - in epicentre) is given in Table 2. The application of the anisotropic model changed the hypocentre depths, on average by 196 metres, with a maximum shift of 558 meters; the average shift of epicentres is 254 meters, the maximum shift is 832 meters. Moreover, the epicentres are shifted systematically towards and away from the seismic network centre, respectively, in the low velocity direction (N-S) and in the high velocity direction (E-W). It must be noted that the shifts of hypocentres are significantly larger for events located outside than for those located inside the network.

In non-linear multiparameter optimization, as in our case, the problem of error estimation is an important but very difficult task. One of the approaches commonly used is to compute a set of the near-optimal solutions. We take the set of solutions which show travel-time residuals better than optimal solution plus 10%. The set of possible anisotropy curves for rays travelling in the horizontal plane is given in Fig. 7.

5. DISCUSSION AND CONCLUSIONS

The geological structure in West Bohemia is rather complex. Therefore, the proper representation of the upper crust medium would be a 3D anisotropic model. In spite of

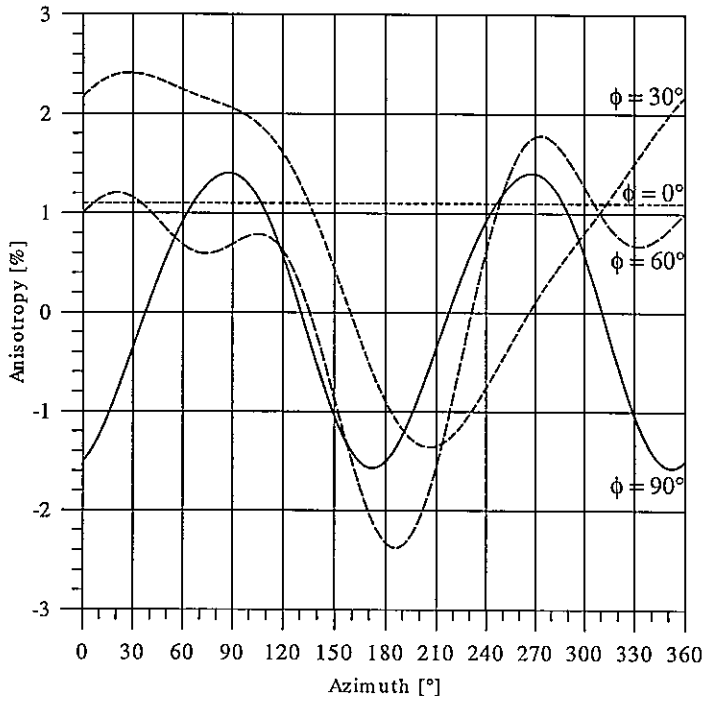

Fig. 6. Azimuthal dependence of anisotropy of the P-wave velocity for four incidence angles.

a large quantity of the data available, we are not able to construct any, more realistic 3D isotropic model. The main reason is that majority of hypocentres is concentrated in very narrow volume at similar depths and thus only the central part of the seismogenic region is sufficiently covered by rays. The 1D isotropic P- and S-wave and even anisotropic qP-wave velocity models adequate up to depth of 15 km that we derived in this study, are a simplification of the real P-wave velocity distribution, nevertheless, they are sufficient to match the observed travel times from controlled sources and arrival times from local earthquakes rather well. Nevertheless, the model derived is worthwhile, because (i) provides an intrinsic estimation of the anisotropy of the upper crust in the region and (ii) approximates very well the upper crust structure for both absolute and relative hypocentre location and approximates, as well as for calculating the response of the medium (Green's function).

Models exhibit much higher P- and S-wave velocity gradients at depths from the surface down to 2.5 km ($\gamma_1 = 4.073$ km/s/km, $\gamma_2 = 0.215$ km/s/km, $\xi_1 = 2.390$ km/s/km, $\xi_2 = 0.200$ km/s/km) in comparison with those at depths between 2.5 and 15 km ($\gamma_3 = 0.049$ km/s/km, $\gamma_4 = 0.047$ km/s/km and $\xi_3 = 0.0017$km/s/km, $\xi_4 = 0.027$ km/s/km).

As follows from Table 1, our isotropic model point out a decrease of the v_p/v_s ratio with depth from 1.70 to 1.63 in the second layer (depths between 0.41 km and 2.46 km) and an increase of the v_p/v_s ratio with depth from 1.63 to 1.70 in the third layer (depths

Table2. Differences in location in isotropic and anisotropic models.

No.	Δr [km]	$z_{ani}-z_{iso}$ [km]	No.	Δr [km]	$z_{ani}-z_{iso}$ [km]
1	0.109	−0.107	34	0.077	−0.165
2	0.257	−0.189	35	0.014	0.163
3	0.129	0.126	36	0.162	0.099
4	0.278	0.349	37	0.287	−0.424
5	0.263	0.303	38	0.228	−0.003
6	0.128	0.191	39	0.213	−0.306
7	0.301	0.080	40	0.245	0.174
8	0.022	−0.015	41	0.171	0.155
9	0.123	0.082	42	0.832	0.218
10	0.085	−0.140	43	0.314	0.025
11	0.100	−0.018	44	0.182	0.063
12	0.143	−0.139	45	0.095	0.049
13	0.304	−0.015	46	0.185	−0.124
14	0.096	−0.305	47	0.235	0.472
15	0.099	−0.035	48	0.154	−0.023
16	0.270	0.118	49	0.100	−0.078
17	0.231	−0.011	50	0.540	−0.032
18	0.327	−0.183	51	0.304	0.293
19	0.043	0.228	52	0.360	−0.380
20	0.047	0.265	53	0.784	0.558
21	0.138	0.218	54	0.402	0.127
22	0.397	−0.228	55	0.260	0.089
23	0.327	0.551	56	0.551	0.353
24	0.269	0.416	57	0.308	−0.317
25	0.107	0.084	58	0.360	0.430
26	0.263	−0.341	59	0.450	0.183
27	0.085	0.075	60	0.189	0.476
28	0.559	0.093	61	0.429	−0.087
29	0.116	−0.065	62	0.527	0.344
30	0.291	−0.154	63	0.138	−0.223
31	0.198	0.382	64	0.242	−0.066
32	0.461	0.387	65	0.179	0.030
33	0.417	0.345			

between 2.46 km and 8.41 km). The v_p/v_s ratio increase can be explained by compositional changes, but it also might be due to the presence of fluid-filled cracks or fractures which results in the v_s decrease. This idea is also supported by the theory of fluid presence of *Špičák and Horálek (2000)*. However, the v_p/v_s ratio increase with depth cannot be considered as fully proven, due to the small number and higher errors of the S-wave onset times.

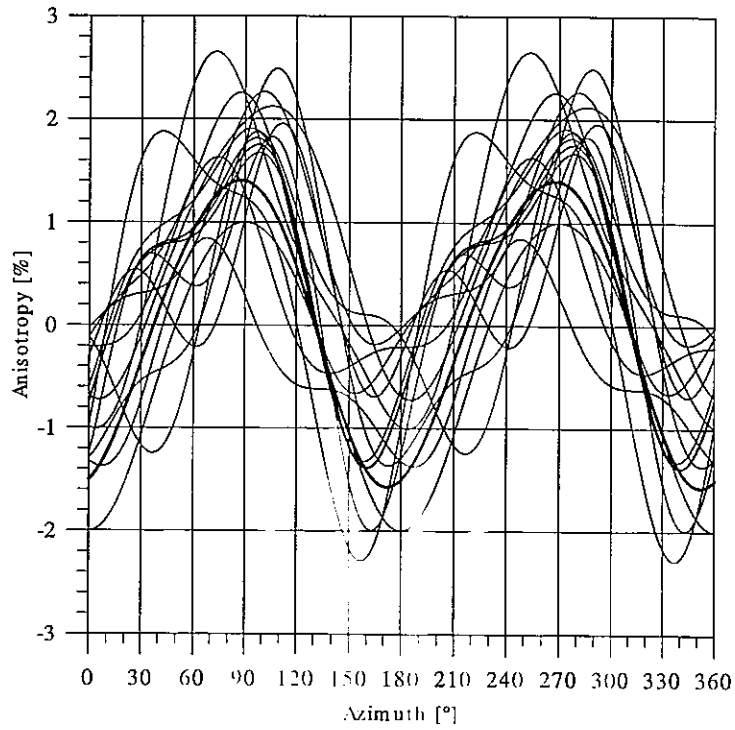

Fig. 7. Estimation of the error of anisotropy in the horizontal plane. The optimum solution is depicted by bold line. All other solutions obtained during the inversion, which display an average residuum smaller or equal to the optimum + 10%, are denoted by thin lines.

The qP-wave velocity model shows 5% P-wave anisotropy. The direction of the lowest velocity in the horizontal plane is oriented nearly in the N-S direction (at an azimuth of 170°). Open question has been a cause of the anisotropy. The stress tensor estimations by means of the focal mechanism inversion show the NW-SE (*Wirth et al., 2000; Havíř, 2000; Plenefisch and Klinge, 2003*) or NNW-SSE (*Sommeitner, 1993; Dahlheim et al., 1997; Havíř, 2000*) orientation of the maximum horizontal axis of compression in the upper crust in the West Bohemia/Vogtland region. A uniform NNW-SSE maximum horizontal stress orientation was also found in the KTB deep borehole based on the breakouts and drilling induced fractures (*Brudy et al., 1997*). Moreover, the paleostress study by *Špičáková et al. (2000)* indicates NNW-SSE direction of the maximum horizontal stress during the Pliocene. Presuming the NNW-SSE principal horizontal stress orientation, the axis of compression is roughly parallel with low velocity direction and perpendicular to high velocity direction. Thus, one of the possible explanations, at least for near surface anisotropy, could be of dipping sedimentary layers which are deformed by the long-term acting stress tensor along the compression axis. Hence, seismic waves propagating throw deformed layers are slower.

The proposed P-wave anisotropy does not have strong influence on location, the shift of the hypocentres in our isotropic and anisotropic models is several hundreds of metres. An accuracy of the location in the isotropic model is, therefore, sufficient for many purposes, e.g., for preliminary location and for source mechanism estimation. The anisotropic model is of a great importance only in specific cases, e.g., in foci migration studies, since foci of the individual swarms cluster in extremely narrow volumes (a few hundreds of metres in diameter), see *Fischer and Horálek (2000), Fischer and Horálek (2003)* and *Janský and Málek (2004).*

The application of the anisotropic model decreases the average P-wave residual only by 19%. This decrease is mainly due to the improvement of the residuals of the travel times from the controlled sources (the first data set). The residuals from local earthquakes (the second data set) are improved only negligibly, being compensated by the shift of hypocentres.

We compared our isotropic velocity model with (a) the WB95 (*Novotný, 1996*) (b) MWE-90 (East) profile (*Behr at al., 1994*) models, and (c) with *Vavryčuk's (1993)* results derived from S-wave splitting in local earthquake seismograms.

(a) A comparison with *Novotný's (1996)* WB95 model (composed of homogeneous layers) is depicted in Fig. 5. The differences between our isotropic P-wave and the WB95 models are mainly due to the high v_p velocity at the Earth's surface (4.6 km/s), and to the existence of several velocity jumps at the layer boundaries in WB95, nevertheless, both of these models evince the same general trends. As an independent test, the location of the January 1997 microearthquake swarm (which occurred in Focal Zone 1) by grid search (*Janský et al., 2000*), was performed in the WB95 model and in our isotropic model. The average residua (both P- and S-onset times) was 86.4 ms for WB95 and 27.8 ms for our isotropic model.

(b) The P-wave velocity models derived from the MVE-90 (East) DEKORP profile data *Behr et al. (1994)*, compared with our isotropic model, display much higher v_p velocities at and near to the Earth's surface (v_p = 5.6 km/s at the surface and $v_p \approx 5.7$ km/s at a depth of 1 km) and much lover P-wave velocity vertical gradient (γ= 0.03 km/s/km) which is constant from surface down to 25 km. The velocity depth function derived from the supplementary 1*R*/90 profile, which was located north-northeast of the area under study, indicates the v_p velocities of 5.7 km/s and 6.1 km/s at depths of 4.0 km and 14.5 km, respectively. These velocities correspond fairly well to those of our minimum velocity model (see Fig. 5); the average P-wave velocity gradient γ= 0.042 also agrees with our results quite well. However, velocity near the Earth's surface v_p = 5.5 km/s seems to be too high similarly as in the MVE-90 (East) model.

(c) The directions of the slowest and fastest P-wave velocities in the horizontal plane do not correspond to those of the S-wave velocities found by *Vavryčuk (1993)* based on S-wave splitting in local earthquake seismograms. The average azimuth of the slow axis in the horizonthal plane found by *Vavryčuk (1993)* was 31°, in the present study the minimal velocity in the horizonthal plane is in the direction 170°, so the difference is 41°. This can be explained by the fact that *Vavryčuk (1993)*

used different stations, which cover smaller area then in the present paper. In both papers the anisotropy is assumed to be constant with depth and also laterally. In reality, the variation of anisotropy could be significant. In the present paper, the anisotropy is strongly affected by data from blasts, which correspond mostly to anisotropy in the uppermost several kilometres, while Vavryčuk's result is an average value from approximately ten kilometers. Finally, the errors of determination in both method are in the order of tens of degrees, so the disagreement can be explained also by low accuracy of the results.

We want to emphasize that the results concerning the anisotropic qP-wave velocity model are valid provided that a perturbation of observed P-wave travel times are due to a real upper crust anisotropy. It cannot be ruled out, however, that the anisotropy obtained in fact compensates for the 3D structure but we are not able to discriminate between the anisotropy and 3D heterogeneity on the basis of our data. Nevertheless, rough estimation has been obtained from the CELEBRATION 2000 and SUDETES 2003 seismic refraction experiments (*Guterch et.al., 2003*) where two long profiles (CEL 09 and S1) and one short profile (R) (*Málek et al., 2001*) crossed at the same shot point Otročín (Φ = 50.021°, Λ = 12.909 °) located about 30 km S-E apart from the West Bohemia earthquake swarm region. Preliminary results show that the effects of anisotropy and 3D heterogeneities of the upper crust on the P-wave travel time perturbations are comparable. However, for a more reliable discrimination between anisotropy or 3D velocity heterogeneity, or the existence of both phenomena, more data are necessary.

Acknowledgements: Our special thanks are due to Alena Boušková for precisely extracting the onset times from the WEBNET seismograms. We are very grateful to Václav Bucha for creating and managing the data base of the shots. The paper benefited greatly from valuable suggestions and constructive remarks by Ivan Pšenčík; his help is gratefully acknowledged. Our special thanks are due to Robert L. Nowack and two anonymous reviewers for their criticism of the original manuscript and for valuable suggestions that helped improve it. The financial support of the Grant Agency of the Czech Republic under Grant No. 205/02/0381 "Complex Geophysical Research in the Seismogenic Western Part of the Bohemian Massif" is gratefully acknowledged.

APPENDIX A
DESCRIPTION OF P-WAVE PHASE VELOCITY IN A WEAKLY ANISOTROPIC MEDIUM

A 1D qP-wave velocity model is represented by the equation:

$$V(z,\phi,\theta)=\alpha(z)\Big[1+\varepsilon_z n_3^4+2n_3^3\left(\varepsilon_{34}n_2+\varepsilon_{35}n_1\right)$$
$$+n_3^2\left(\delta_x n_1^2+\delta_y n_2^2+2\chi_z n_1 n_2\right)+2n_3\left(\chi_x n_1^2 n_2+\chi_y n_1 n_2^2+\varepsilon_{15}n_1^3+\varepsilon_{24}n_2^3\right)$$
$$+\varepsilon_x n_1^4+\delta_z n_1^2 n_2^2+\varepsilon_y n_2^4+2\varepsilon_{16}n_1^3 n_2+2\varepsilon_{26}n_1 n_2^3\Big].$$

Here, $V(z,\phi,\theta)$ is qP-wave velocity in an anisotropic medium, α denotes isotropic P-wave velocity(the background model), z is a depth, ϕ is an azimuth ($0 \le \phi \le 2\pi$), θ is a

polar angle $(0 \le \theta \le \pi)$, $n = (n_1, n_2, n_3) = (\cos\phi\cos\theta, \sin\phi\sin\theta, \cos\theta)$ is the phase propagation direction; ε, δ, and χ are defined by *Pšenčík and Gajewski (1998)* as follows:

$$\varepsilon_x = \left(A_{11} - \alpha^2\right) \Big/ \left(2\alpha^2\right),$$

$$\varepsilon_y = \left(A_{22} - \alpha^2\right) \Big/ \left(2\alpha^2\right),$$

$$\varepsilon_z = \left(A_{33} - \alpha^2\right) \Big/ \left(2\alpha^2\right),$$

$$\delta_x = \left(A_{13} + 2A_{55} - \alpha^2\right) \Big/ \alpha^2,$$

$$\delta_y = \left(A_{23} + 2A_{44} - \alpha^2\right) \Big/ \alpha^2,$$

$$\delta_z = \left(A_{12} + 2A_{66} - \alpha^2\right) \Big/ \alpha^2,$$

$$\chi_x = \left(A_{14} + 2A_{56}\right) \Big/ \alpha^2,$$

$$\chi_y = \left(A_{25} + 2A_{46}\right) \Big/ \alpha^2,$$

$$\chi_z = \left(A_{36} + 2A_{45}\right) \Big/ \alpha^2,$$

$$\varepsilon_{15} = A_{15} \Big/ \alpha^2,$$

$$\varepsilon_{16} = A_{16} \Big/ \alpha^2,$$

$$\varepsilon_{24} = A_{24} \Big/ \alpha^2,$$

$$\varepsilon_{26} = A_{26} \Big/ \alpha^2,$$

$$\varepsilon_{34} = A_{34} \Big/ \alpha^2,$$

$$\varepsilon_{35} = A_{35} \Big/ \alpha^2,$$

where A_{11} to A_{66} are general anisotropy parameters in Voigt's notation.

APPENDIX B
ISOMETRIC INVERSE ALGORITHM

Isometric Method (IM) is a fast algorithm, which was developed for solving weakly non-linear inverse problems with many parameters. The basic idea is to transform the Euclidien distance in that way that the model space and the data space are isometric (for

definition see bellow) and to transfer the representation of the misfit vector from data space to model space (see bellow).

The measured quantities are called the data and form the data space. The number of the data is n. One realization of measurement defines one vector, d, in the data space of dimension n. The errors of measurement are expressed in the form of a covariance matrix:

$$C_{ij} = E\left(\left(d_i - E\left(d_i\right)\right)\left(d_j - E\left(d_j\right)\right)\right), \tag{B-1}$$

$E(x)$ being the expectance of quantity x.

The scalar product $d_1 \cdot d_2$ and distance $v_D\left(d_1, d_2\right)$ in the data space are defined in usual form:

$$d_1 \cdot d_2 = \sum_{ij} d_{1i} C_{ij} d_{2j}\ ,\ v_D\left(d_1, d_2\right) = \sqrt{\sum_{ij}\left(d_{1i} - d_{2i}\right) C_{ij}\left(d_{1j} - d_{2j}\right)}, \tag{B-2}$$

d_{xi} being the components of data vector d_x, $i = 1, \ldots, n$.

The model is described by model parameters, which form the model space. Each vector of the model space p with dimension m represents one model. Data and model parameters are related by equations, which describe the forward problem:

$$d = F\left(p\right). \tag{B-3}$$

The goal of the inverse problem is to select the "optimum" model; it means a model closest to the measured data in the sense of the distance in the data space. The idea of the IM is to define the distance between two models in the model space v_M as the distance of their function values in the data space. This distance is herein defined as:

$$v_M\left(p_1, p_2\right) = v_D\left(F\left(p_1\right), F\left(p_2\right)\right). \tag{B-4}$$

This definition means that the model space and data space are isometric (which gave name to the whole method). Such defined distance is invariant with respect to the change of parameterization.

Many inverse algorithms (including IM) employ linearization to increase the convergence efficiency. As such, they work better if the forward problem is nearly linear. It is very advantageous to chose the parameterization p_i in such manner that the forward problem is only weakly non-linear. However, there is no general rule how to achieve this.

In IM, $m + 1$ vectors of model parameters and corresponding $m + 1$ data vectors are kept in memory at every moment (Fig. B1). The best model and corresponding data vector closest to the measured data in the current time are designated p_b and d_b, the other supporting vectors are designated $p_1 \ldots p_m$ and $d_1 \ldots d_m$. The worst model from supporting vectors and corresponding data vector are designated p_w and d_w. Models are generated randomly at the beginning of the computation. Sometimes, it is possible to obtain starting model. In that case, this model is accepted as p_b and only models $p_1 \ldots p_m$ are randomly generated.

The misfit vector M is in IM introduced as the difference between the measured data d_M and the best data vector d_b:

$$M = d_M - d_b \,. \tag{B-5}$$

The norm of the misfit vector $\|M\|$ has to be minimized. In the IM, unlike in most of inverse algorithms, the problem is not reduced to the minimization of this scalar misfit. Instead, the complete misfit vector is taken into account. However, the misfit $\|M\|$ is also used in the IM. If the misfit is defined in the model space $\|M\|(p)$, we speak about a misfit function.

The misfit vector can be approximated with the aid of other m auxiliary vectors $\boldsymbol{a}$:

$$a_i = d_i - d_b \,. \tag{B-6}$$

To achieve this, constants $c_1 \ldots c_m$ must be found to minimize the balance vector $\boldsymbol{B}$:

$$B = M - \sum_i c_i a_i \;,\; i = 1 \ldots m \,. \tag{B-7}$$

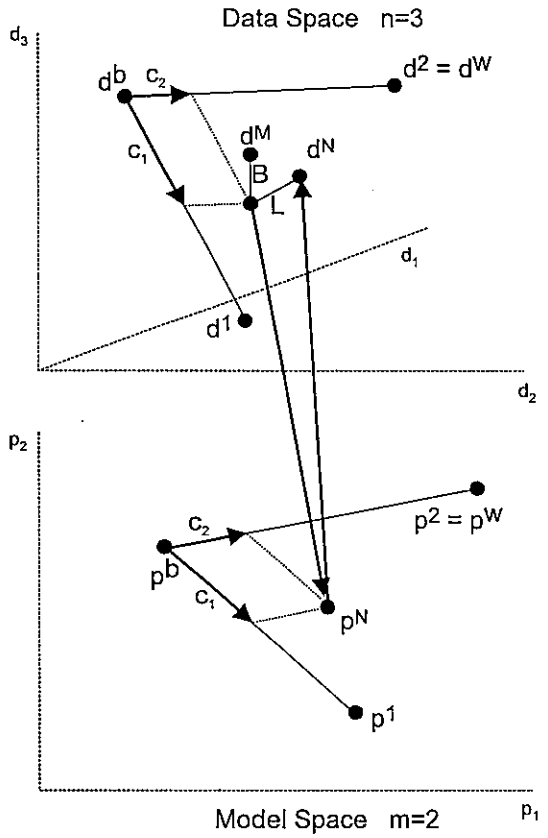

Fig. B1. Isometric method for simple case $m = 2$, $n = 3$.

Note the meaning of the balance vector $\boldsymbol{B}$. The norm of the balance vector $\|B\|$ is the distance of the measured data from hyperplane h (of order m) in the data space (of dimension n). The procedure of finding c_i involves projection of the misfit vector to the hyperplane h and its subsequent decomposition to the directions of auxiliary vectors $\boldsymbol{a}_i$. This is a classical linear inverse problem, which can be solved by a number of methods. The most usual is the Newton's method of least squares. In the Newton's method, however, a system of linear equation of order m must be solved; if the determinant of this system is small, the solution is not stable. For this reason in IM the method of single parameter approximation is used instead. That means that the misfit vector is projected to the first auxiliary vector $\boldsymbol{a}_1$ and thus decomposed into two components: component $\acute{c}_1\boldsymbol{a}_1$ parallel to $\boldsymbol{a}_1$ and the residual perpendicular component r. The same procedure is performed with component r and vector $\boldsymbol{a}_2$, and so on. After $\boldsymbol{a}_m$, we start again with $\boldsymbol{a}_1$, values of $\acute{c}_i$ from the individual iterations are summed and converge to constants c_i. After several iterations, component r is nearly perpendicular to all auxiliary vectors, the solution is reached. One of the advantages of this method is the absence of the need to solve a system of linear equations (the projection is realized by computation of a scalar product). The principal advantage is, however, that constants c_i can be easily kept within certain limits, for instance within interval $(-1, 2)$. If these limits are introduced, vector $\sum c_i a_i$ is no longer an exact projection of $\boldsymbol{M}$ to hyperplane h. But on the other hand, the vector $\boldsymbol{d}_B + \sum c_i a_i$ is close to vectors $\boldsymbol{d}_B$, $\boldsymbol{d}_1 \ldots \boldsymbol{d}_m$ and it is very advantageous in case of strongly non-linear forward problem. The choice of these limits will be discussed later.

As soon as constants c_i are obtained, a new model $\boldsymbol{p}_N$ can be composed in the model space as:

$$\boldsymbol{p}_N = \boldsymbol{p}_b + \sum c_i \left(\boldsymbol{p}_i - \boldsymbol{p}_b\right). \tag{B-8}$$

The corresponding data vector can be also composed

$$\boldsymbol{d}_N = F\left(\boldsymbol{p}_N\right). \tag{B-9}$$

If the forward problem $F(\boldsymbol{p})$ is linear, it is obvious that

$$\boldsymbol{d}_N = \boldsymbol{d}_b + \sum c_i \left(\boldsymbol{d}_i - \boldsymbol{d}_b\right) = \boldsymbol{d}_M - \boldsymbol{B}. \tag{B-10}$$

Therefore, $\boldsymbol{p}_N$ is the solution of the inverse problem. In non-linear problems, it is very likely that $\boldsymbol{d}_N$ is closer to the measured data $\boldsymbol{d}_M$ than $\boldsymbol{d}_b$. Two vectors useful in further computation are herein defined:

step vector $$\boldsymbol{S} = \boldsymbol{d}_N - \boldsymbol{d}_b, \tag{B-11}$$

and vector of linearity $$\boldsymbol{L} = \boldsymbol{d}_N - \boldsymbol{d}_B - \sum c_i a_i. \tag{B-12}$$

Vector $\boldsymbol{L}$ is zero in the case of a linear problem. The relation $\|L\| > \|B\|$ indicates that the non-linearity is strong: in the next iteration, it is recommended to make stricter the limits for c_i. In the opposite case, if $\|L\| < \|B\|$, the non-linearity is not so strong and the

limits can be remitted. The best convergence can be achieved if $\|L\| \approx \|B\|$. These vectors are of course strongly dependent on the current supporting vectors. It is therefore necessary to be careful and use the values from several successive iterations for the determination of limits. In most cases this strategy speeds up the convergence significantly.

Vector S has the meaning of the step from the old solution to the new one. It is used as an indicator of progress during the computation. If too small, it may suggest that a solution was found, but it may also mean that the choice of the supporting vectors was not good. In that case, it is recommended to substitute some supporting vectors before going any further.

If the new model d_N is closer to the d_M than the worst supporting vector d_w, then d_N should be accepted as one of the supporting vectors and the worst supporting vector should be omitted. If d_N is closer than d_b, the two vectors should be interchanged. Then, it should be continued with the next iteration. So, only one forward problem computation is normally needed per iteration.

If the new model d_N has the longest distance from d_M of all supporting vectors (it could happen in case of strong non-linearity), it should be rejected. Then the worst supporting vector is omitted and the next step is a random search (see bellow). If step $\|S\|$ is very small, it is recommended to leave only the best model p_b and generate new generation of supporting vectors.

If some vectors were omitted, new vectors must be added to the number of $m + 1$. This is done by random generating in the vicinity of the best model p_b. The limits for random search are increased or decreased during the generation to make the distance of the newly generated vector p_N from the best model p_b comparable with the misfit of the best model $\|M\|(p_b)$. Only such new vector should be adopted, which meets the condition:

$$v_M(p_N, p_b) < 2\|M\|(p_b) \tag{B-13}$$

A new model p_N better than p_b can be sometimes found during this random search. In that case, these two should be interchanged. Finding an optimum solution could be virtually achieved only by this random search, because intervals for the random search becoming smaller every time a new model p_b is found, as implied from equation (B-13). Nevertheless, the isometric algorithm is much faster. So, as soon as the number of supporting vectors reaches $m + 1$, the algorithm continues with misfit vector approximation (B-7).

The iteration continues until the criteria for stopping are met. These criteria are based on values $\|M\|$ and $\|S\|$. If $\|S\|$ becomes very small in several successive iterations and the change of the supporting vectors proves ineffective, the computation should be stopped. The value of the final $\|M\|$ can be roughly estimated. It is herein designated as M_F. It was found empirically, that in most cases, a good estimation is

$$M_F \approx \sqrt{(n-m)}\,. \tag{B-14}$$

A criterion for stopping the procedure can be thus formulated: the misfit $\|M\|$ did not improve in the last m iterations, and, the misfit $\|M\|$ is close to M_F, or $\|S\|$ is very small in the last m iterations.

It should be stressed once more that this criterion is not strictly defined and one should be careful about obtaining the best solution. A good strategy is to repeat the inversion several times.

The above described isometric algorithm connects the advantages of several commonly used methods (*Tarantola, 1987*).

IM employs linearization of the forward problem as the Newton's least squares method. This produces high efficiency in cases of weak non-linearity (linear cases are solved immediately in the first iteration). But the Newton's method employs a matrix of derivatives: this is computed again in each iteration, which is time-consuming. Instead, IM uses differences between supporting vectors (which can be used in many successive iterations) to meet the same purpose. The use of differences emphasizes the global aspects of the misfit function, while the derivatives emphasize some local aspects.

IM keeps the population of $m+1$ models in memory, like the simplex method; however, the method of finding a new model is completely different to the simplex method.

The new models are in some cases chosen randomly but always only in the vicinity of the best model. The intervals for this random search are defined by misfit of the best model and, as such, they become smaller during the computation. This resembles the method of simulated annealing. The main advantage of this approach is the limited risk of finding a local minimum of the misfit function instead of the global one.

In spite of the fact that the IM shares features of several well-known methods, it represents a complex method, where all parts are needed. To some extent, it may reflect the non-linearity of the problem, with random search being utilized more often in cases of a stronger non-linearity. Nevertheless, it is not designed for solving problems with really strong non-linearity. In such cases, it is recommended to change the parameterization of the problem in such way that it becomes more linear.

The common method used for the estimation of errors of the optimum model is the computation of a covariance matrix in the model space. However, in case of multiple model parameters, this approach is not ideal mainly for two reasons:

Computation of the covariance matrix is time-consuming: it may take even more computer time than finding of the optimum model.

In case of a large number of parameters and non-linear problems, the covariance matrix is not sufficient for the description of errors. The covariance matrix corresponds to derivatives of the second order of the misfit function at the point of the minimum. The misfit function is, however, often very complex and the second derivatives approximate the misfit function only in a small area around the minimum, which is not sufficient for error estimation.

This is why the IM employs a different approach to error estimation. During computation, "successful" models are stored on the disk together with their misfit vectors. Successful models are those having a shorter distance from the d_M than a certain constant, for instance $3\sqrt{(n-m)}$. If the set of successful models is too small at the end of the

computation, a larger number of models can be randomly generated in the vicinity of the solution. The errors can be roughly estimated from this set of models. A condition for this approach is a sufficiently large set of successful models. Most of them are computed during the optimization process; however, the distribution of the parameters is not equal. It is therefore recommended to generate a larger number of models at the end of the optimization process in the neighborhood of the optimum model.

References

Babuška V. and Plomerová J., 1987. Deep tectonics of the lithosphere in western part of the Bohemian Massif. In: D. Procházková (Ed.), *Earthquake Swarm 1985/86 in Western Bohemia.* Geophys. Inst. of Czechosl. Acad. Sci., Prague, Czech Rep., 30–33.

Behr H.J., Dürbaum H.J. and Bankwitz P. (Eds.), 1994. Crustal structure of the Saxothuringian zone: Results of the deep seismic profile MVE-90 (East). *Z. Geol. Wiss.*, **22**, 647–769.

Bräuer K., Kämpf H., Strauch G. and Weise S.M., 2003. Isotopic evidence ($^3He/^4He$, $13C_{CO2}$) of fluid-triggered intraplate seismicity. *J. Geophys. Res.*, **108**, 2070, doi: 10.1029/2002JB002077.

Brudy M., Zobak M.D., Fuchs K., Rummel F. and Baumgärtner J, 1997. Estimation of the complete stress tensor to 8 km depth in the KTB scientific drill holes: Implication for crustal strengs . *J. Geophys. Res.*, **102(B8)**, 18453–18475.

Bucha V. and Blížkovský M., 1994. *Crustal Structure of the Bohemian Massif and the West Carpathians.* Academia, Prague, Czech Rep.

Dahlheim H.A., Gebrande H., Schmedes E. and Soffel H., 1997. Seismicity and stress field in the vicinity of the KTB location. *J. Geophys. Res.*, **102(B8)**, 18493–18506.

Fischer T., 2003. The August-December 2000 Earthquake swarm in NW Bohemia: the first results based on automatic processing of seismograms. *J. Geodyn.*, **35**, 59–81.

Fischer T. and Horálek J., 2000. Refined locations of the swarm earthquakes in the Nový Kostel focal zone and spatial distribution of the January 1997 swarm in Western Bohemia, Czech Republic. *Stud. Geophys. Geod.*, **44**, 210–226.

Fischer T. and Horálek J., 2003. Space-time distribution of earthquake swarms in the principle focal zone of the NW Bohemia/Vogtland seismoactive region: Period 1985-2001. *J. Geodyn.*, **35**, 59–81.

Guterch A., Grad M., Špičák A., Brückl E., Hegedüs E., Keller G.R., Thybo H. and CELEBRATION 2000, ALP 2002, SUDETES 2003 Working Groups, 2003: An overview of recent seismic refraction experiments in Central Europe. *Stud. Geophys. Geod.*, **47**, 651–657.

Havíř J., 2000. Stress analyses in the epicentral area of Nový Kostel (western Bohemia). *Stud. Geophys. Geod.*, **44**, 210–226.

Heinicke J. and Koch U., 2000. Slug flow - a possible explanation for hydrochemical earthquake precursors at Bad Brambach, Germany. *Pure Appl. Geophys.* **157**, 1621–1641.

Horálek J., Fischer T., Boušková A. and Jedlička P., 2000. Western Bohemia/Vogtland region in the light of the WEBNET network. *Stud. Geophys. Geod.*, **44**, 107–125.

Janský J., 1969. Refracted wave in a horizontally stratified medium with constant velocity gradients. *Stud. Geophys. Geod.*, **13**, 423–443.

Janský J., Horálek J., Málek J. and Boušková A., 2000. Homogeneous velocity models of the West Bohemian swarm region obtained by grid search. *Stud. Geophys. Geod.*, **44**, 158–174.

Janský J. and Málek J., 2004. Relocation of earthquakes in West Bohemian/Vogtland subregions Lazy, Klingenthal and Plesná using Master event method. *Acta Geodynamica et Geomaterialia*, **1**, No.4, 73–83.

Klimeš L., 1995. Examples of seismic models. In: *Seismic Waves in Complex 3-D Structures*, Report 3, Dept. of Geophys., Faculty of Math. and Phys., Charles University, Prague, Czech Rep.

Málek, J. 1997. *Interpretation of Seismograms from Local Seismic Networks*. PhD Theses, Charles University, Prague, Czech Rep. (in Czech).

Málek J., Janský J. and Horálek, J., 2000. Layered velocity models of the Western Bohemia region. *Stud. Geophys. Geod.*, **44**, 475–490.

Málek J., Brož M., Fischer T., Horálek J., Hrubcová P., Janský J., Novotný O., Růžek B. and the CELEBRATION Working Group, 2001. Seismic measurements along short profiles in western Bohemia during the CELEBRATION 2000 experiment. *Acta Montana IRMS AS CR*, Series A, No.18, 15–28.

Málek J., Janský J., Novotný O. and Rössler D., 2004. Vertically inhomogeneous models of the upper crustal structure in the West-Bohemian seismoactive region inferred from the CELEBRATION 2000 refraction data. *Stud. Geophys. Geod.*, **48**, 709–730.

Mrlina J., 2000. Vertical displacement in the Nový Kostel seismoactive area. *Stud. Geophys. Geod.*, **44**, 336–345.

Neunhöfer H. and Güth D., 1989. Detailed investigation of the great earthquake swarm in Western Bohemia by local Vogtland network. In: P. Bormann (Ed.), *Monitoring and Analysis of the Earthquake Swarm 1985/86 in the Region Vogtland/Western Bohemia*. Akad. der Wissensch. der DDR, Potsdam, Germany, 124–164.

Novotný O., 1996. A preliminary seismic model for the region of the West-Bohemian earthquake swarms. *Stud. Geophys. Geod.*, **40**, 353–366.

Novotný O., Janský J. and Málek J., 2004: Some aspects of application of the Wiechert-Herglotz method to refraction data from western Bohemia *Acta Geodynamica et Geomaterialia*, **1**, No.2, 157–164.

Plenefisch T. and Klinge K., 2003. Temporal variations of focal mechanisms in the Novy Kostel focal zone (Vogtland/NW Bohemia) - comparison of the swarms of 1994, 1997 and 2000. *J. Geodyn.*, **35**, 145–156.

Pšenčík I. and Gajewski D., 1998. Polarization, phase velocity, and NMO velocity of qP-waves in arbitrary weakly anisotropic media. *Geophysics*, **63**, 1754–1766.

Sonnleitner M., 1993: *Vergleich unterschiedlicher Methoden der Spannungsinversion von Erdbebendaten - am Beispiel von Erdbeben aus der Region Vogtland/westl. Böhmen.* Diploma Thesis, Institut für Allgemeine und Angewandte Geophysik der Ludwig-Maximilians-Universität München, München, Germany.

Špičák A., 2000. Earthquake swarms and accompanying phenomena in intraplate regions: A review. *Stud. Geophys. Geod.*, **44**, 89–106.

Špičák A. and Horálek J., 2000. Possible role of fluids in the process of earthquake swarm generation in the West Bohemia/Vogtland seismoactive region. *Tectonophysics*, **336**, 151–162.

Špičáková L., Uličný D. and Koudelková G., 2000. Tectonosedimentary evolution of the Cheb Basin (NW Bohemia, Czech Republic) between late Oligocene and Pliocene. A preliminary note. *Stud. Geophys. Geod.*, **44**, 556–580.

Švancara J., Gnojek I., Hubatka F. and Dědáček K., 2000. Geophysical field pattern in the West Bohemia geodynamic active area. *Stud. Geophys. Geod.*, **44**, 307–326.

Tarantola A., 1987. *Inverse Problem Theory*. Elsevier Science B.V, Amsterdam, The Netherlands.

Vavryčuk V., 1993. Crustal anisotropy from local observations of shear-wave splitting in West Bohemia, Czech Republic. *Bull. Seismol. Soc. Am.*, **83**, 1420–1441.

Wirth W., Plenefisch T., Klinge K., Stamler K. and Seidel D., 2000. Focal mechanisms and stress field in the region Vogtland/Western Bohemia. *Stud. Geophys. Geod.*, **44**, 126–141.